Chapitre 5

On the geophysical information captured by MIPAS limb infrared emission profiler

C. De Clercq[1], J.-C. Lambert[1], and T. von Clarmann[2]

[1]Belgian Institute for Space Aeronomy (IASB-BIRA), Belgium
[2]Forschungszentrum Karlsruhe, Institut für Meteorologie und Klimaforschung (FZK-IMK), Germany

Published in GEOMON Technical Note.
De Clercq, C., J.-C. Lambert, and T. von Clarmann, GEOmon D4.2.1 - Chapter 2 : Multidimensional characterisation of satellite measurements of infrared emission at limb, Tech. Rep. TN-IASB-GEOMON/SECPEA, Issue 1, Revision B, BIRA-IASB, 9 March 2009.

Sommaire

Après notre étude de l'instrument UV-visible à visée nadir GOME, nous nous intéressons, dans ce chapitre, à une technique de mesure différente, basée sur l'émission infrarouge au limbe. Nous étudions en particulier les mesures de l'instrument MIPAS (Michelson Interferometer for Passive Atmospheric Sounding). Contrairement aux mesures au nadir, la visée au limbe permet d'obtenir des profils atmosphériques avec une haute résolution verticale. Leur résolution horizontale est par contre limitée par la longueur du chemin optique tangent à l'atmosphère et doit être prise en compte dans de nombreuses applications. Nous proposons ici de caractériser l'information réellement mesurée dans le plan de sondage de l'instrument MIPAS et de déterminer sa résolution horizontale. Nous développons également des outils qui permettront aux utilisateurs des données MIPAS de prendre en compte cette résolution horizontale dans des applications comme l'assimilation, la validation et l'étude de tendance.

Ce travail a été réalisé dans le cadre des projets GEOmon (Global Earth Observation and Monitoring of the Atmosphere) financé par la Commission Européenne (EC) et ProDEx SECPEA (Space-based Exploration of the Chemistry and Physics of the Earth's Atmosphere) . *Comme évoqué dans l'introduction générale, le projet GEOmon vise la mise en place au niveau européen d'un système global de surveillance de l'atmosphère et constitue un premier pas vers la mise en*

place du GEOSS. Le projet regroupe différentes activités. L'activité 1 concerne les gaz à effet de serre, l'activité 2 la pollution de l'air, l'activité 3 les aérosols, l'activité 4 l'ozone stratosphérique, l'activité 5 la modélisation et l'assimilation des données et l'activité 6 la communication et l'information au monde politique et scientifique et au public. L'activité 4 comprend l'acquisition des mesures de l'ozone stratosphérique depuis le sol (WP 4.1), l'intégration des données GEOmon avec les observations des satellites (WP 4.2) et l'étude des tendances à long terme de l'ozone, de la température, du dioxyde d'azote et du monoxyde de brome (WP 4.3). Notre contribution au projet s'inscrit dans le cadre de cette activité et plus précisément du WP 4.2. Elle consiste en une caractérisation de mesures issues de différentes techniques de télédétection. Un des objectifs est de déterminer la résolution horizontale des mesures satellitales dans les domaines IR, visible et UV et pour des géométries de visée au limbe, en occultation ou au nadir. Ce travail est fortement lié aux autres activités du projet GEOmon. Nous développons des outils et méthodes permettant d'améliorer l'assimilation des observations dans les modèles prévision numérique (Activité 5), la validation géophysique et l'étude de tendances à long terme (W.P 4.3) en prenant en compte les caractéristiques réelles de l'information sondée. Le projet SECPEA, coordonné par l'IASB, complète ces études GEOMon avec une tâche dévolue plus particulièrement à l'assimilation des observations satellitales dans les modèles de prévision et d'analyse numérique de la composition de l'atmosphère.

La caractérisation de la résolution horizontale des mesures satellitales en émission infrarouge, appliquée à l'instrument MIPAS/Envisat présentée ici constitue le deuxième chapitre d'une note technique du projet GEOmon [De Clercq et al., 2009]. Le chapitre 1 étudie la résolution horizontale des instruments au sol [J.-C. Lambert] et les suivants porteront sur d'autres techniques satellitaires. Dans un premier temps, nous étudions la radiance mesurée par l'instrument MIPAS. Ce travail a été réalisé à l'IASB à l'aide d'un modèle de transfert radiatif infrarouge simplifié développé dans ce but [De Clercq and Lambert, 2006b]. Dans un second temps, nous prenons en compte le modèle d'inversion. Lors de cette étude, réalisée en collaboration avec Thomas von Clarmann et ses collègues du FZK-IMK à Karlsruhe (Allemagne), j'ai pu passer une semaine à l'IMK pour utiliser leur modèle de transfert radiatif KOPRA. Cette partie des résultats a été publiée dans le journal Atmospheric Measurement Techniques (AMT) [von Clarmann et al., 2009].

The limb radiance of MIPAS

C. De Clercq[1], J.-C. Lambert[1], and T. von Clarmann[2]

[1]Belgian Institute for Space Aeronomy (IASB-BIRA), Belgium
[2]Forschungszentrum Karlsruhe, Institut für Meteorologie und Klimaforschung (FZK-IMK), Germany

First part of GEOMON Technical Note - D4.2.1 - Chapter 2: Multi-dimensional characterisation of satellite measurements of infrared emission at limb (9 March 2009).

5.1 Introduction

Remote sensing of the atmospheric limb from orbiting platforms yields access to information on the vertical distribution of atmospheric species at high vertical resolution, typically in the range of 1-3 km. It is a common practice of limb data users to assume that the retrieved information concentrates around the tangent point. Implicitly, this common practice assumes that the horizontal smearing of information is negligible and that the centroid - or barycentre - of the retrieved quantity does not deviate noticeably from the tangent point. In accordance with this assumption, typical limb sounding retrieval schemes also assume local horizontal homogeneity of the atmosphere, i.e. the vertical profile of temperature and of atmospheric species is retrieved under the (usually hard-wired) assumption that the atmosphere probed during one limb scan varies only with altitude but not horizontally [*McKee et al.*, 1969; *Mill and Drayson*, 1978; *Goldman and Saunders*, 1979; *Carlotti*, 1988; *Ridolfi et al.*, 2000; *von Clarmann et al.*, 2003, e.g.,].

In reality, the horizontal resolution achievable by sounders measuring the limb infrared (IR) emission is physically limited by a combination of radiative processes, including competing emissions and absorptions, which occur along optical paths of several hundred kilometres, and on properties of the limb scanning sequence, of the instrument (e.g., the field of view), and of the orbit. Consequently, it might happen that the centroid and the tangent point are distant by hundreds of kilometres, and that the retrieved information spreads significantly around the centroid, moreover in preferred directions determined by the limb scanning sequence and by instrumental and orbital properties. The spread and the actual position of the centroid determine the smoothing properties of the measurement system.

As in the vertical direction, any kind of smoothing of horizontal atmospheric structures can generate the so-called horizontal smoothing error [*Rodgers*, 1990, 2000], an error depending on the existence of atmospheric inhomogeneities. This error is inherent to both the measurement system and the retrieval scheme and cannot be dissociated from their combination. When comparing

observational data with different horizontal smoothing properties, e.g., for satellite validation purposes, and when comparing observational data with modelled data, e.g. in a chemical data assimilation process, differences in smoothing properties must be considered appropriately. In the case of atmospheres horizontally homogeneous at the scale of the air mass probed by the satellite, neglecting the actual difference in resolution leads to sub-optimal collocation criteria for validation and under-constraining observation operators for data assimilation. Where inhomogeneities of the atmosphere occur in the preferred directions of the satellite observation and at scales comparable with its horizontal resolution, neglecting the difference in horizontal smoothing of atmospheric homogeneities adds, to the individual measurement and retrieval errors characterising each data set, the so-called smoothing error [*Rodgers*, 1990, 2000]. In cases of large atmospheric inhomogeneities, the comparison error due to smoothing differences can even exceed the individual error bars of each data set and make meaningless the bias and scatter derived from the comparison.

In this chapter we propose an original study of the horizontal information content of atmospheric composition profiles retrieved from limb IR emission spectra. Since properties of the retrieved information vary with the species and with parameters like the scanning sequence and the spectral microwindows, the study focuses on Michelson Interferometer for Passive Atmospheric Sounding (MIPAS, [*Fischer et al.*, 2008]) on board of Envisat, the only European limb IR sensor operating in the time period of the project, and on its target species: CO_2 (temperature retrieval), H_2O, O_3, CH_4, $N2O$, HNO_3, and NO_2. In the first part of this study (*"Analysis of MIPAS limb radiance"*), using a simplified radiative transfer model, we explore the information accessible by the measurement technique by quantifying spectroscopic and geometric phenomena controlling the radiance signal reaching the satellite, independently of the retrieval technique. In the second part (*"The horizontal resolution of MIPAS"*), we study the information content obtained by coupling the measurement system with the retrieval system. The horizontal - or better, angular - component of two-dimensional averaging kernels of a limb retrieval constraint to horizontal homogeneity is calculated, using the IMK KOPRA radiative transfer forward model and an unconstrained global fit approach similar to that used in the operational MIPAS data processor [*Carlotti*, 1988]. Based on the Rodgers formalism [*Rodgers*, 1990, 2000], the horizontal averaging kernels show how the system smoothes departure of the a-priori profile from the true atmospheric profile and characterise the horizontal resolution of a full retrieval system (forward and inverse model). They may serve as observation operators for data assimilation and validation. The conclusion (*"General conclusion and recommendations"*) discusses the results and draws general recommendations for limb infrared emission profile data users.

5.2 The MIPAS instrument

Since 2002, the European Space Agency's (ESA) environmental satellite (Envisat) is flying, on a quasi-polar (inclination of 98.6°) sun-synchronous orbit at mean altitude of 800 km. Every 100 min, it crosses the descending node at the mean solar time of 10:00 am. The Envisat atmospheric chemistry payload includes the Michelson Interferometer for Passive Atmospheric Sounding (MIPAS) instrument [*Fischer et al.*, 2008]. MIPAS is a cooled, high resolution Fourier Transform Spectrometer designed for the detection of limb emission spectra in the middle and upper atmosphere. Four spectral channels cover the middle infrared spectral range from 650 cm^{-1} to 2400 cm^{-1} at, in its original measurement mode which was operational until March 2004, about 0.025 cm^{-1} resolution (unapodized), allowing the detection of large set of atmospheric species.

From July 2002 to March 2004, the MIPAS interferometer was operated in the nominal resolution mode. The instrument registers limb emission spectra in a backward viewing along track geometry. A small azimuth angle between the pointing direction and the along track direction is adjusted along the orbit to maximize the coverage and allow measuring atmospheric profiles over the Poles. The instrumental field of view at the tangent point is of about 3 km vertically by 30 km across-track. A complete limb-scanning sequence spans vertically the atmosphere from 68 km down to 6 km in tangent altitude, with a vertical spacing between successive measurements of 3 km in the troposphere and stratosphere and a coarser spacing above. In March 2004, the instrument incurs a major anomaly and the operations were stopped. The anomaly was identified as a failure of the mirror sliding mechanism on one of arms of the Michelson interferometer. The MIPAS operation could be resumed in a reduced resolution mode in February 2005. Vertical distributions of pressure, temperature and mixing ratio of six high-priority species (O_3, H_2O, HNO_3, CH_4, N_2O and NO_2) were retrieved from MIPAS Nominal Resolution spectra by the operational data processors developed under ESA's responsibility [*Ridolfi et al.*, 2000; *Raspollini et al.*, 2006]. Most of current algorithms do not take into account potential two-dimensional effects. Profile retrieval algorithms are based on multiple line fitting in a set of optimised spectral microwindows [*Dudhia et al.*, 2002] and on the global fit approach [*Carlotti*, 1988]. With this particular approach, the one-dimensional vertical profile of a given species is retrieved from the simultaneous analysis of all spectral measurements acquired during an entire limb-scanning sequence.

5.3 Limb-scanning sequence and orbital progression

Within the angular plane in which the MIPAS instrument registers limb emission spectra, a complete limb-scanning sequence spans vertically the atmosphere from high to low altitudes between 68 km and 6 km in tangent altitude. During an entire limb-scanning sequence, the same atmospheric layer is intersected several times by different optical paths. Downward scanning is associated with a retrograde motion of tangent points with respect to the satellite, of about 1.1 degree between the upper (at 68 km) and lowest (at 6 km) tangent points of the sequence. Moreover, the satellite itself orbits in the opposite direction at a speed of about 7.45 km/s. At the end of a complete sequence (72.213 s), the satellite has progressed of 4.28 degree along its orbit. Taking into account the azimuth angle between the orbital plane and the pointing direction, all these contributions result in a net angular spacing of about 2.45 degree, varying slightly with latitude, between the upper and lowest tangent points of the sequence. Figure 5.1 sketches the resulting geometry for four successive MIPAS limb scan elements.

In nominal mode, the MIPAS instrument registers limb emission spectra in a backward viewing geometry. The azimuth mirror provides access to any limb target rearwards within a 35° wide range around the anti-flight direction. To enable a full polar coverage, the azimuth angle is set as a sinusoidal function of the time along the orbit (see illustration in Figure 2). Further applications will need a precise identification of the angular plane in which the MIPAS instrument registers limb emission spectra. Unfortunately this information is not provided in the MIPAS data files. However, it can be either calculated from the Envisat orbit parameters or extracted from auxiliary files of the onboard DORIS positioning system.

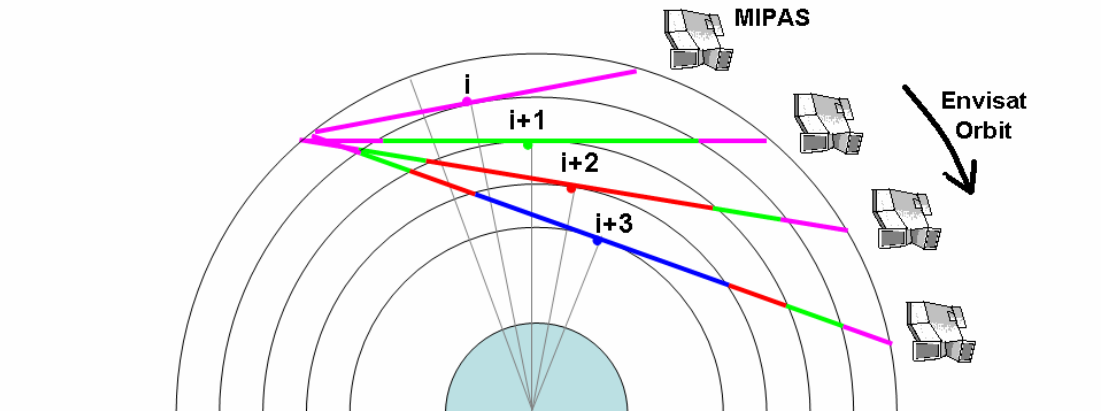

Figure 5.1: Geometrical illustration of the information sounded by MIPAS during four successive limb measurements (tangent altitudes i down to $i+3$) in backward viewing mode. Successive tangent points follow the orbital progression of Envisat. The atmospheric layer between tangent points i and $i+1$ is intersected by all individual scans from tangent altitude $i+1$ down to the lowest tangent altitude.

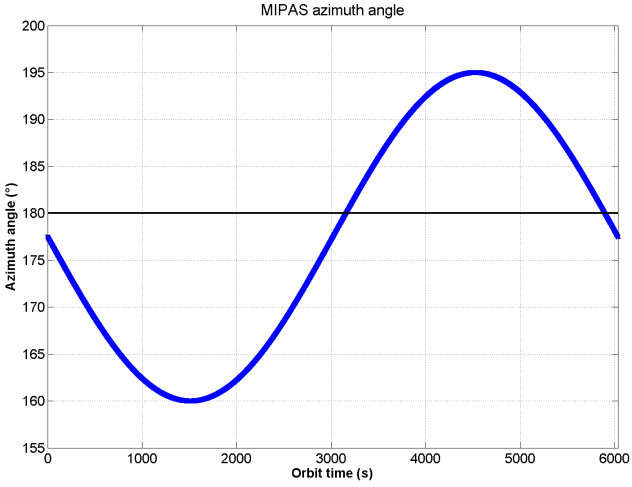

Figure 5.2: Azimuth angle between the orbital plane and the MIPAS line-of-sight as a function of time along the orbit.

5.4 Simplified radiative transfer model

Before taking into account effects of the retrieval method, the first step to determine the angular distribution of the measured information within a complete IR limb-scanning sequence is to investigate the physical phenomenon at the source of and controlling the detected signal. Spectra measured by MIPAS results from emissions and absorptions competing along the long optical paths. At infrared wavelengths, Rayleigh scattering in the upper troposphere and higher can be neglected. To understand the two-dimensional contribution to total radiance, we have developed a simplified radiative transfer model to calculate monochromatic limb radiances. In this simplified model, refraction and Mie scattering by clouds and aerosols are neglected. Nor does this model take into account MIPAS instrumental parameters, like spectral instrument response function, vertical field of view.

5.4.1 Radiative transfer basics

Radiative transfer basics resemble those adopted for operational MIPAS data processing [*Carlotti et al.*, 1998; *Fischer et al.*, 2000; *Ridolfi et al.*, 2000]. Infrared radiance spectra L in $W/(m^2.sr.m^{-1})$ emitted and absorbed at wave number ν (cm^{-1}) by a given molecule along the limb optical path s, are calculated for an observer $Obs.$ using Eq. 5.1,

$$L_{\nu,Obs.}(ztg) = \int_{Obs.}^{-\infty} k_\nu(s_{tg}) B_\nu(T(s_{tg})) e^{\left(-\int_{Obs.}^{s_{tg}} k_\nu(x_{tg}) dx_{tg}\right)} ds_{tg} \tag{5.1}$$

where s_{tg} and x_{tg} are line-of-sight coordinates along the optical path with tangent point altitude z_{tg}. B_ν is the spectral radiance emitted by Planck's black body source at temperature T.

5.4.2 Calculation of the absorption cross section

The absorption cross sections of each species are calculated from the molecule spectroscopic parameters refers in the high-resolution molecular absorption database HITRAN2004 [*Rothman et al.*, 2005]. A simple line-by-line algorithm is used to calculate the cross sections in various microwindows (MW). Here, we have used the same microwindows than those used by *Ceccherini* [2004] for the calculation of vertical averaging kernels and listed in Table 5.1.

The absorption cross section of one molecular species k_ν (m^{-1}) is obtained by summation over all lines of the species:

$$k_\nu = \sum_{l=1}^{lines} L_l A_l(\nu - \nu_l, T, p) \tag{5.2}$$

where L_l is the intensity and A_l is the line-shape at temperature T and pressure p of line l. ν_l is the central wavenumber of line l.

The line intensity can be derived from the high-resolution molecular absorption database HITRAN2004 using the formula:

$$L_l = L(T_0) \frac{Q(T_0)}{Q(T)} \frac{e^{\frac{-hcE}{kT}}}{e^{\frac{-hcE}{kT_0}}} \frac{(1 - e^{\frac{hc\sigma}{kT}})}{(1 - e^{\frac{hc\sigma}{kT_0}})} \tag{5.3}$$

where $L(T_0)$ is the line strength at reference temperature T_0, and E'' is the lower state energy of the transition that are directly obtained from the HITRAN2004 database. $Q(T)$ and $Q(T_0)$ are the total internal partition functions at temperature T and at reference temperature T_0 (296K). k is the Boltzmann constant and c is the light velocity.

The line shape is a Voigt profile, i.e. the convolution of the Doppler and the Lorentz profile. The Voigt profile can be written as the real part of the error function:

$$A_l = \sqrt{\frac{ln2}{\pi}} \frac{1}{a_D} \Re(erf(z)) \tag{5.4}$$

where z is a complex given by:

$$z = \sqrt{ln2} \left(\frac{\nu - \nu_l}{a_D} + i \frac{a_L}{a_D} \right) \tag{5.5}$$

a_D and a_L are, respectively, the full with at half maximum (FWHM) of the Doppler and the Lorentz profile. They can be calculated from HITRAN2004 parameters as:

$$a_D = \nu_l \sqrt{2ln2 \frac{kT}{Mc}} \tag{5.6}$$

$$a_L = a_L^0 \frac{p}{p_0} \left(\frac{T_0}{T} \right)^{\gamma_l} \tag{5.7}$$

where M is the molecular mass of the species, a_L^0 is the Lorentz half width at reference temperature T_0 and reference pressure p_0 (101325 Pa) and γ_l is the coefficient of temperature dependence of the half width.

5.4.3 Ray tracing model

The radiative transfer integral (Eq. 5.1) is a curvilinear integral along the line-of-sight, determined by the viewing direction of the instrument and by the refractive index of the air. The bending of the optical path due to refraction was not considered in this simplified radiative transfer model.

A geometrical ray tracing should be performed to determine the relation between satellite coordinate - geometrical distance from tangent point (x) and tangent altitude (z_{tg}) - and Earth centred coordinates - angular distance from tangent point (ϕ) and Earth centred altitude (r). Along each optical path this relation could be expressed by:

$$r = \sqrt{x^2 + (z_{tg} + R_t)^2} - R_t \tag{5.8}$$

$$\phi = arctg \left(\frac{x}{z_{tg}} \right) \tag{5.9}$$

The altitudes z and z_{tg} are here expressed with reference to the centre of the Earth. These equations correspond to the polar coordinate change, which Jacobian is given by:

$$\frac{\partial(\phi, r)}{\partial(x, z_{tg})} = r \tag{5.10}$$

The effect of satellite motion can be added at this stage. As discussed previously, the net effect is an angular spacing of about 2.45 degree in the orbit plane between the upper and lowest

tangent points of the sequence. This is taken into account as an additional coordinate change in the mapping:

$$\phi\prime = \phi + a(z_{tg} - z_0) \tag{5.11}$$

where a is the net angular spacing between the upper and lowest tangent points of the sequence ($a = 2.45°/62$ km for MIPAS). The Jacobian of the second coordinate change is given by:

$$\frac{\partial \phi\prime}{\partial \phi} = 1 + a\frac{\partial z_{tg}}{\partial \phi} = 1 + arsin\phi \tag{5.12}$$

Figure 3 gives a schematic view of the two performed coordinate change and of the ray tracing.

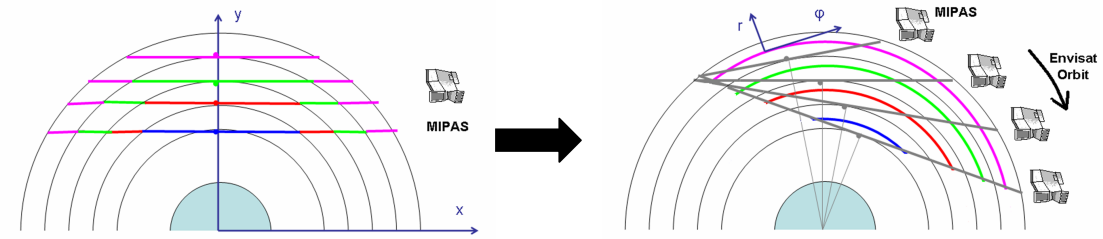

Figure 5.3: Schematic view the change of coordinate, from satellite centred coordinate (s, z_{tg}) to Earth-centred coordinate (r, ϕ), included in the ray tracing algorithm.

5.5 Two-dimensional modelling of MIPAS radiance

5.5.1 Synthetic spectra

The radiative transfer model described at section 5.4 has been run to simulate the vertical sequence of limb radiance spectra of each absorber and for all spectral microwindows listed in Table 5.1. The atmosphere is modelled as a compilation of 120 concentric and homogeneous layers, extending from the ground up to the top of atmosphere (TOA) fixed at 120 km. Typical concentration profiles of the target species were selected from documented sources such as the AFGL atmospheric profile database [*Anderson et al.*, 1986], the COSPAR International Reference Atmosphere CIRA [*Fleming et al.*, 1990; *Keating et al.*, 1996], and the URAS Reference Atmosphere Project URAP, adapted by *Kiefer et al.* [2002] for MIPAS retrieval purposes. Figure 5.4 displays the selected profiles of O_3,H_2O, HNO_3, CH_4, N_2O, NO_2 and CO_2.

Figure 5.5 shows, as example, limb radiances calculated at a selection of tangent altitudes from 68 km to 6 km for O3 profile retrieval in MW1 and MW3. These synthetic spectra reproduce correctly known features as, for example, the broadening of emission lines when the pressure increases.

Table 5.1: Spectral and altitude range of the microwindows (MW) used in the simplified radiative transfer model.

		Spectral range (cm^{-1})	**Altitude range (km)**
PT(CO_2)	MW 1	685.700-685.825	33-47
	MW 2	686.400-689.400	30-68
	MW 4	694.800-695.100	27-36
	MW 5	700.475-701.000	21-30
	MW 6	728.300-729.125	15-27
	MW 7	741.975-742.250	15-24
	MW 8	791.375-792.875	6-33
H_2O	MW 1	807.850-808.450	12-18
	MW 2	946.650-947.700	6-18
	MW 3	1645.525-1646.200	27-60
	MW 4	1650.025-1653.025	15-68
O_3	MW 1	763.375-766.375	6-68
	MW 2	1039.375-1040.325	52-68
	MW 3	1122.800-1125.800	6-68
N_2O	MW 2	1233.275-1236.275	6-27
	MW 6	1272.050-1275.050	12-60
CH_4	MW 1	1227.175-1230.175	6-60
	MW 4	1350.875-1353.875	12-68
NO_2	MW 1	1607.275-1610.275	15-68
	MW 2	1613.725-1616.600	15-68
	MW 4	1622.550-1623.475	6-30
HNO_3	MW 1	876.375-879.375	6-68
	MW 2	885.100-888.100	6-42

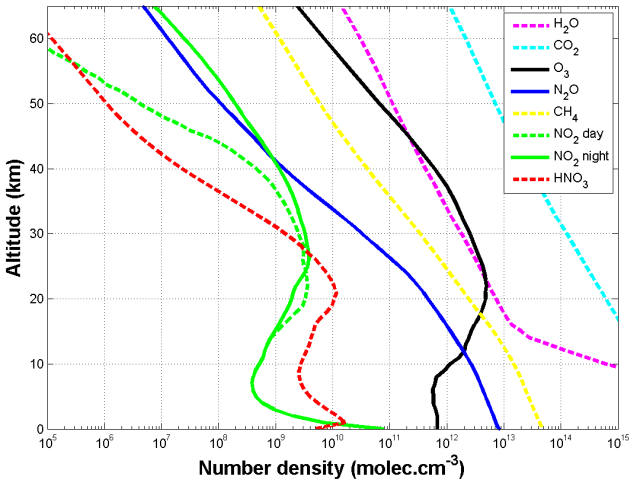

Figure 5.4: Typical vertical profiles of the concentration of O_3, H_2O, HNO_3, CH_4, N_2O, NO_2 and CO_2. These profiles are used to run the simplified radiative transfer model.

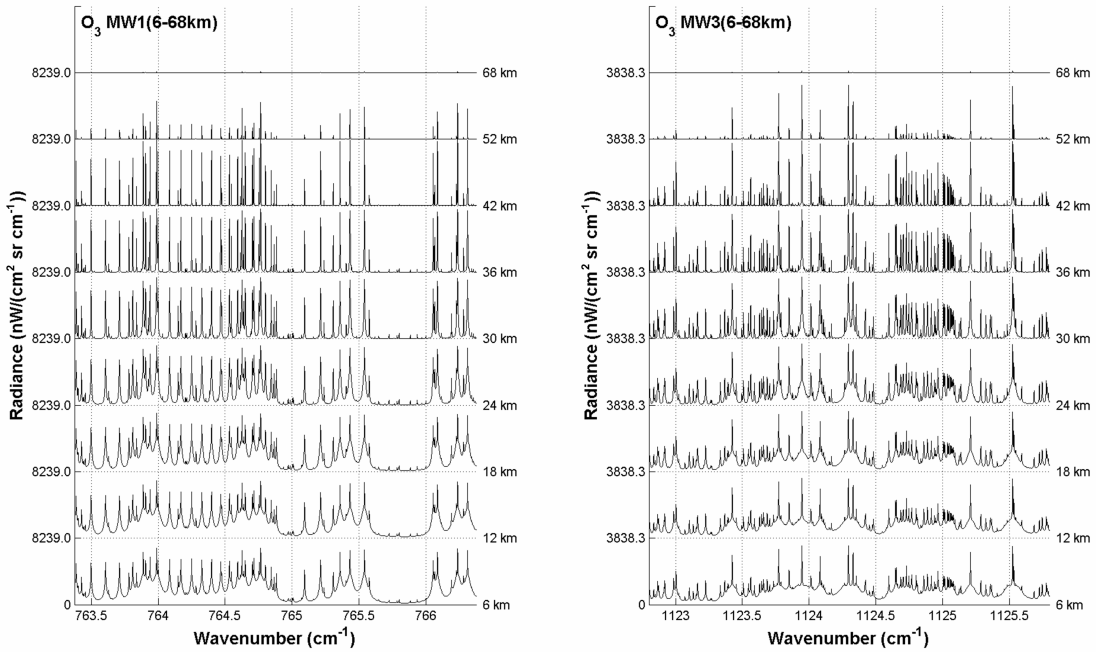

Figure 5.5: O3 radiances measured during a MIPAS limb-scanning sequence (tangent point sampling the limb at altitudes from 68 km down to 6 km) in microwindows 1 (left) and 3 (right).

5.5.2 Line-of-sight contribution to radiance

The spectral contribution in $W/(m^2.sr.m^{-1}.m)$ of each line-of-sight element (ds_{tg}) to the total spectral radiance received by the observer ($Obs.$) is given by the integrant of Eq. 5.1:

$$dL_{\nu,Obs.}(z_{tg}) = k_\nu(s_{tg})B_\nu(T(s_{tg}))e^{\left(-\int_{Obs.}^{s_{tg}} k_\nu(x_{tg})dx_{tg}\right)}ds_{tg} \tag{5.13}$$

The two first terms of this product correspond to the local emission of element d_{stg} while the last term correspond to the absorption occurring between the emitter and the satellite.

By integrating this expression along the wavelength for the entire micro-windows, we obtain the total contribution in W/(m2.sr.m) of one element of the optical path to the total radiance :

$$dL_{Obs.}(z_{tg}) = \int_{MW} k_\nu(s_{tg})B_\nu(T(s_{tg}))e^{\left(-\int_{Obs.}^{s_{tg}} k_\nu(x_{tg})dx_{tg}\right)}ds_{tg}d\nu \tag{5.14}$$

Figure 6 displays the contribution to the total CO_2 radiance in MW2 and MW8 as a function of the tangent altitude. At this stage, geometrical ray tracing effects are not taken into account yet. The line-of-sight contribution to radiance shows, for the two microwindows, a displacement of information toward the satellite. Contribution of each optical path element to the total radiance for N_2O, CH_4 and H_2O bears a similar shape than that of CO_2. However, the exact form of the contribution function varies from one molecule to another and from one microwindow to another. Figure 7 displays the same contribution function as obtained for O_3 total radiance in MW1. The contribution function is similar to that obtained for CO_2, however below 20 km a double maximum pattern appears. It corresponds to the double crossing of the maximum concentration layer during limb scanning at low tangent altitudes. A similar double maximum pattern is observed for NO_2 and HNO_3 which are also trace gases with a stratospheric maximum of concentration. For all molecules, the contribution of atmospheric layers located far from the satellite is the smallest. Indeed, the light emitted beyond the tangent point is more absorb along the longer optical path toward the satellite.

5.5.3 Angular contribution to radiance

Using ray tracing and associated change of coordinates, defined at section 3.2.1 (including satellite motion), we express the contribution to the total radiance in Earth-centred space, as a function of altitude and angular distance from tangent point (i.e., optical path/tangent altitude coordinates become angular distance/retrieval altitude coordinates). To be representative of the global fit retrieval algorithm, our approach considers the radiances measured during an entire limb-scanning sequence as a continuous 2-dimensional function:

$$dL_{Obs.}(\phi\prime, r) = dL_{Obs.}\left(s_{tg}(\phi\prime, r), z_{tg}(\phi\prime, r)\right)\frac{\partial(s_{tg}, z_{tg})}{\partial(\phi, r)}\frac{d\phi}{d\phi\prime} \tag{5.15}$$

$$= dL_{Obs.}\left(s_{tg}(\phi\prime, r), z_{tg}(\phi\prime, r)\right)\frac{r}{1 - ar\sin\phi} \tag{5.16}$$

The obtained functions represent the horizontal contribution of each atmospheric layer to the MIPAS total radiance within the different microwindows. To obtain a unique set of contribution functions for each molecule, the contributions from the individual microwindows are further added (whithin the altitude ranges defined in the retrieval algorithm, see Table 5.1). Figure 5.8 shows

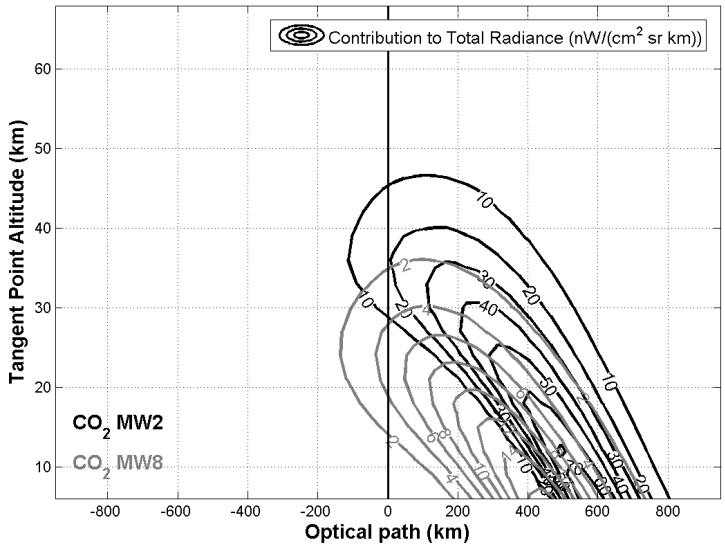

Figure 5.6: Line-of-sight contribution to the CO_2 limb radiance (in $W/cm^2.sr.km$) calculated in MW2 and MW8, and displayed as a function of tangent altitude and optical path distance from tangent point.

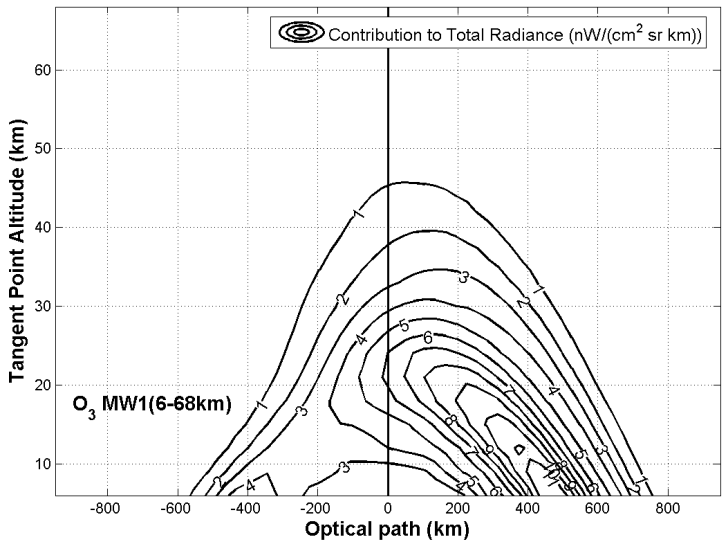

Figure 5.7: Same as Figure 5.6 but for line-of-sight contribution to the O3 limb radiance calculated in MW1.

the obtained results for the six MIPAS target species (O_3, H_2O, HNO_3, CH_4, N_2O, NO_2) and temperature (CO_2). The colour plot shows the contribution of to the total radiance in Earth centred coordinated. The contribution functions, in each altitude level, have been normalized. Grey lines depict the median and the 95% centred quantile distance (CQD) of the contribution to radiance. The x% CQD is the distance between the $x + (1-x)/2$ and the $(1-x)/2$ quantiles and indicates the horizontal region x percent of information originates from. Black line displays the displacement of successive tangent points due to the satellite motion during the full limb sequence.

For all molecules, the angular contributions to radiance are bounded to limited angular extent. For geometrical reasons, the spread increases monotonically with altitude, from 230-400 km at 9 km up to 1300-1700 km at 68 km for 95% of the information. The median displacement varies from -100 to 520 km, depending on the altitude and the molecule. The angular position of the maximum of radiance also varies with altitude and with molecule. At lower altitudes, it is strongly displaced in front of the tangent point toward the satellite. At higher altitudes, the maximum of radiance is still strongly displaced toward the satellite for CO_2, and H_2O; is between the satellite and the tangent point or at the tangent point for O_3 and CH_4; and it is beyond the tangent point for HNO_3, N_2O and NO_2. Light emitted from air volume located further from the satellite is more absorbed along the longer optical path than for light from air volume close to the satellite. Large displacement of the maximum radiance toward the satellite may, then, be understood by a complete re-absorption of radiance emitted near the tangent point in higher atmospheric layers. However absorption depends on various parameters as the gas concentration and temperature of in the crossed atmospheric layers. These effects, combined with geometrical issues, are responsible of the complex shape of the radiance contribution functions. It will be analysed in more detail in following section.

5.6 Shape of contribution to radiance

The shape of the contribution to radiance is quite complex and varies with altitude and with molecule. However some general feature can be highlighted. To better understand complex feature, we study separately three different effects: the spatial extent of the full limb sequence, the competing IR emission and absorption along the line-of-sight and the satellite motion.

5.6.1 Spatial extent of the full limb sequence

The first effect determining the shape of the contribution to radiance is the geometry of a limb scanning sequence. To isolate this effect from other geometrical and physical phenomenons, we consider a homogenous non-absorbing atmosphere and a satellite located at the infinity. In such an atmosphere, within the same altitude layer, the contributions to radiance of each air parcel are identical. Indeed, the local emission depends on temperature and on trace gas concentration that are assumed to be constant within one altitude layer. Figure 5.9 sketches the geometry of the limb sequence and the resulting contribution to radiance in this theoretical case. The upper altitude layer is crossed by all limb scans; while the lowest altitude layer is crossed only by the lowest tangent limb scan. Consequently, the angular portion of an altitude layer that contributes to the total radiance decreases with altitude. The final width of the contributing portion is determined by the altitude of the lowest limb scan. The resulting contributions to radiance are step functions and their widths represent the portion of each atmospheric layer that is seen by the instrument

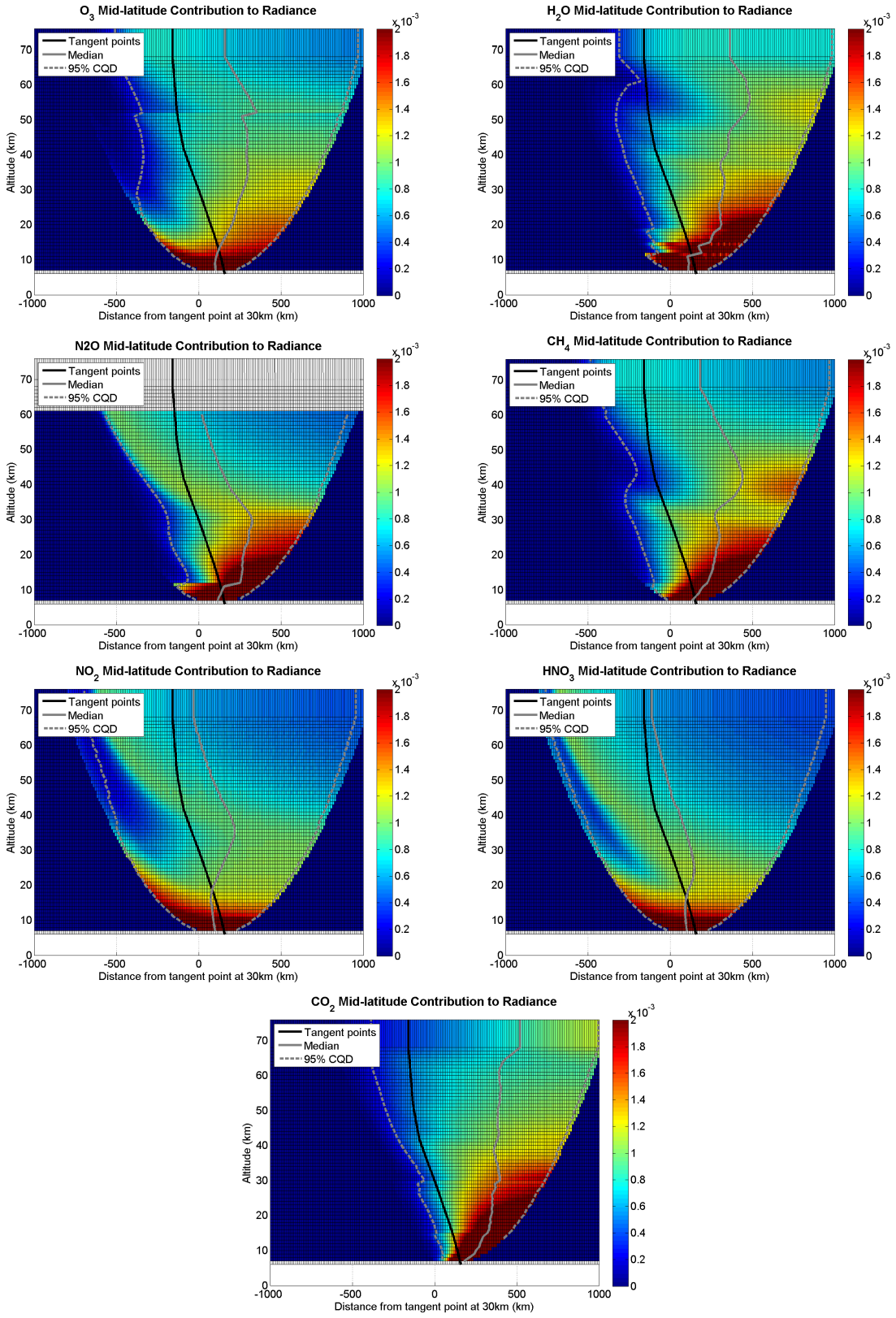

Figure 5.8: Angular contribution to the O_3, H_2O, HNO_3, CH_4, N_2O, NO_2 and CO_2 limb radiance (normalized within each altitude level). Contributions from the various microwindows have been added.

during the full limb sequence. This effect explains why contributions to radiance are all bounded to a limited angular extent increasing with altitude.

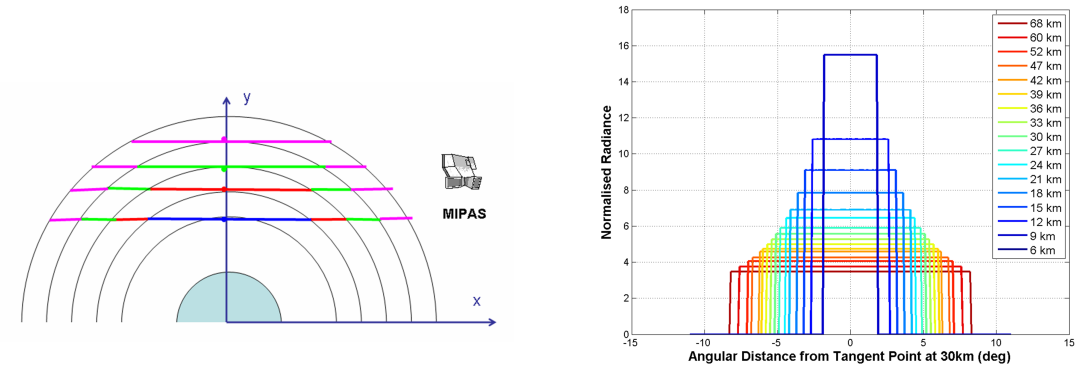

Figure 5.9: Geometry of the limb sequence and resulting contribution to radiance in each altitude layer for a non-absorbing atmosphere and for satellite located at the infinity.

5.6.2 Competing emissions and absorptions along the line-of-sight

The second effect determining the global shape of the contribution to radiance is combining emission and absorption along the optical path. This effect depends on the vertical distribution of the target gas. Two general cases have been distinguishes: (i) the gas concentration decreases with altitude; (ii) the gas concentration present a maximum in the stratosphere. To separate from other geometrical effect the satellite position is still considered as located at the infinity.

Figure 5.10 sketches the emission and absorption processes along one atmospheric layer and resulting contribution to radiance for a gas, like CO_2, H_2O, N_2O and CH_4, which concentration decrease with altitude. Then, the optical thickness of the atmosphere decreases with altitude. Above a certain level, the absorber concentration is very weak and the absorption can be neglected. The optically thick part of the atmosphere is filled in green and parts of the optical path where absorption occurs are highlighted in red. Two cases are distinguished.

First, the considered altitude layer is within the optically thick part of the atmosphere. When moving from close to far from the satellite along this atmospheric layer, the optical path between the emitter and the satellite increases, and consequently absorption increases. At low altitude the resulting the contributions to total radiance are, then, decreasing functions.

Second, the considered altitude layer is outside the optically thick part of the atmosphere. When moving from close to far from the satellite along this atmospheric layer, in a first time the optical path from the emitter to the satellite first does not cross the absorbing layers. The contribution to total radiance is then constant. At further angular distance, the emitting points sets behind the optically tick layers and the absorption reduces progressively the contribution the total radiance. At high altitude the resulting contributions to radiance first stand to a constant value before decreasing to zero.

Figure 5.11 sketches the emission and absorption processes along one atmospheric layer and resulting contribution to radiance for a gas, like O_3, NO_2 and HNO_3, which concentration present a maximum in the stratosphere. At high altitude, the emission and absorption combine in a similar

way than in previous analysis and contribution function have a similar shape. Only for atmospheric layer below or within the optical dense part of the atmosphere the behaviour is different.

For emitters between the satellite and the tangent point, the optical path trough optically thick layer increases with angular distance, and the contribution to total radiance decreases. However, at the other side of the atmosphere, the optical path crosses first non-absorbing layers before crossing the optically dense part of the atmosphere. Consequently, the length of the optical path, where absorption occurs, decreases and the contribution to total radiance increases. A low altitude the contribution to the total radiance decrease when eloigning from the satellite, reaches a minimum and then increase again, without reaching its initial value. This effect explains the minimum in radiance observed at low altitude and large angular distance in O_3, NO_2, and HNO_3 contribution compared to other gases.

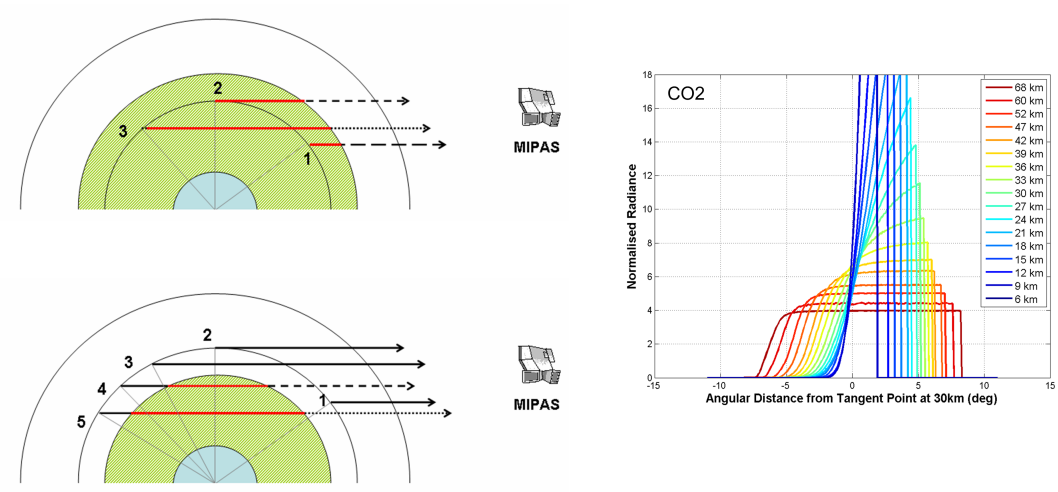

Figure 5.10: Schematic description of the emission and absorption processes along the line-of sight for various points within the same atmospheric layer. The trace gas concentration decreases with altitude and the satellite is located at the infinity. The optically thick part of the atmosphere is colored in green. Parts of the optical path where absorption occurs are highlighted in red. Top: the considered atmospheric layer is outside the optically thick part of the atmosphere. Bottom: the considered atmospheric layer is inside the optically thick part of the atmosphere. Right panel shows the resulting contribution to radiance for a vertical profile of CO_2.

5.6.3 Satellite motion

The third effect acting on the global contribution to radiance is the motion of the satellite during the full limb sequence. To study this effect separately, a non-absorbing homogeneous atmosphere, where the contributions to radiance of each air parcel are identical, is considered. Figure 5.12 sketches the geometry of the limb sequence in such an atmosphere, when the satellite is moving, and resulting contribution to radiance. While a limb sequence of spectra is recorded top down, i.e. from the uppermost to the lowermost tangent altitude, Envisat moves about 510 km in the opposite of the viewing direction. This leads, during one single limb scan, to denser sampling of the

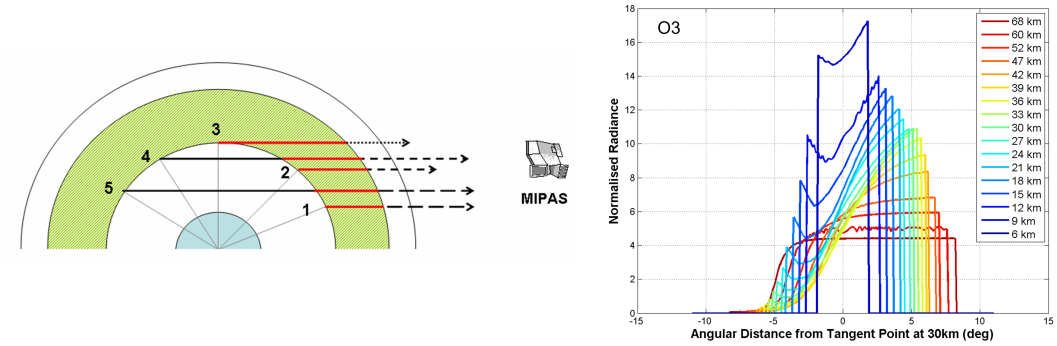

Figure 5.11: Same as Figure 10 but for a trace gas concentration that present a maximum in the stratosphere. The considered atmospheric layer is inside the optically thick band part of the atmosphere. Right panel shows the resulting contribution to radiance for a vertical profile of O_3.

atmosphere beyond the tangent points than satellite-side of the tangent point. As a consequence, the retrieval uses more information per latitude increment from beyond the tangent point. It results in a contribution to the radiance maximum beyond the tangent point and decreasing toward the satellite.

The finite MIPAS field of view, of about 3 km in the vertical at the tangent point, might lead to and additional effect. Beyond the tangent point the fields of view of measurements at adjacent tangent altitudes are overlapping, leading to multiple sampling of air masses beyond the tangent point. This effect might account for a backward displacement of the median point by 1-7 km. However, due to its small amplitude this effect has been neglected.

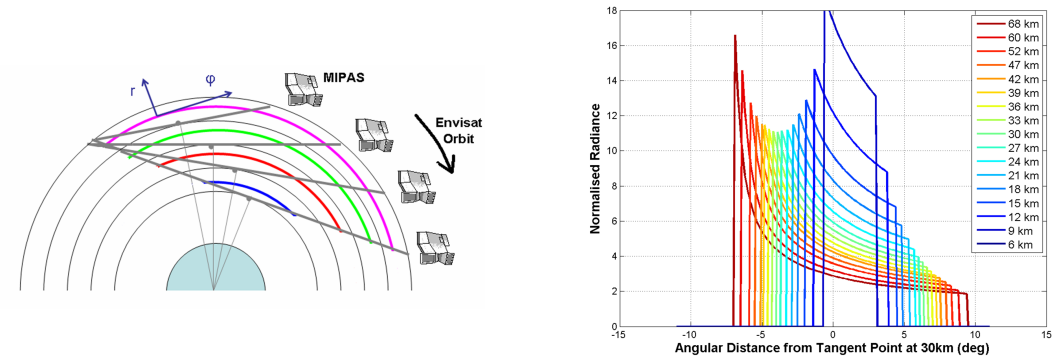

Figure 5.12: Effect of satellite motion on theoretical observation operators for an ideal atmosphere in which the contribution to the total radiance would be constant in each atmospheric layer.

5.7 Conclusion

In this section, we have simulated limb infrared radiance spectra for various molecules to investigate the angular distribution of radiance collected by a limb IR instrument like MIPAS. The study highlights that the radiance measured by MIPAS is not confined to a single point but come from a broad horizontal part of the atmosphere. The horizontal spread of the radiance extends from 230-400 km at 9 km up to 1300-1700 km at 68 km (95% CQD). Moreover the radiance maximum is not located at the tangent point but can be in front or beyond it depending on the altitude and on the molecule. Different concurring effects explain the detail shapes of the contribution to radiance. Emissions and absorptions competing along the long optical paths, give more weight to air masses located between the tangent point and the satellite; while, the progression of the satellite along its orbit add geometrical and dilution effects.

The horizontal information content of the concentration profiles inverted from MIPAS measurement does not depend only from the source of the measured signal but also of the retrieval system. Moreover, the information does not necessarily come from the point where the radiance comes from, but rather depends on the sensitivity of the radiance to a change in the gas concentration (i.e. the derivative of the radiance). Therefore the study of radiance is only a first step to understand the horizontal spread of sounded information and should be complete by an analysis of the output of a real retrieval system. These issues will be studied in the next part of this analysis.

The horizontal resolution of MIPAS

T. von Clarmann[1], C. De Clercq[2], M. Ridolfi[3], M. Höpfner[1], and J.-C. Lambert[2]

[1]Forschungszentrum Karlsruhe, Institut für Meteorologie und Klimaforschung (FZK-IMK),Karlsruhe, Germany
[2]Belgian Institute for Space Aeronomy (IASB-BIRA),Brussels, Belgium
[3]Dipartimento di Chimica Fisica e Inorganica, Università di Bologna, Italy

Published in Atmospheric Measurement Techniques.
von Clarmann et al., The horizontal resolution of MIPAS, Atmos. Meas. Tech., 2, 47-54, 18 February 2009, www.atmos-meas-tech.net/2/47/2009/

Abstract

Limb remote sensing from space provides atmospheric composition measurements at high vertical resolution while the information is smeared in the horizontal domain. The horizontal components of two-dimensional (altitude and along-track coordinate) averaging kernels of a limb retrieval constrained to horizontal homogeneity can be used to estimate the horizontal resolution of limb retrievals. This is useful for comparisons of measured data with modeled data, to construct horizontal observation operators in data assimilation applications or when measurements of different horizontal resolution are intercompared. We present these averaging kernels for retrievals of temperature, H_2O, O_3, CH_4, N_2O, HNO_3 and NO_2 from MIPAS (Michelson Interferometer for Passive Atmospheric Sounding) high-resolution limb emission spectra. The horizontal smearing of a MIPAS retrieval in terms of full width at half maximum of the rows of the horizontal averaging kernel matrix varies typically between about 200 and 350 km for most species, altitudes and atmospheric conditions. The range where 95% of the information originates from varies from about 260 to 440 km for these cases. This information spread is smaller than the MIPAS horizontal sampling, i.e. MIPAS data are horizontally undersampled, and the effective horizontal resolution is driven by the sampling rather than the smearing. The point where the majority of the information originates from is displaced from the tangent point towards the satellite by typically less than 10 km for trace gas profiles and about 50 to 100 km for temperature, with a few exceptions for uppermost altitudes. The geolocation of a MIPAS profile is defined as the tangent point of the middle line of sight in a MIPAS limb scan. The majority of the information displacement with respect to this nominal geolocation of the measurement is caused by the satellite movement and the geometrical displacement of the actual tangent point as a function of the elevation angle.

5.8 Introduction

Typical limb sounding retrieval schemes assume local horizontal homogeneity of the atmosphere, i.e., vertical profiles of atmospheric state variables are retrieved under the (usually hard-wired) assumption that the atmosphere seen during one limb scan varies only with altitude but not in the horizontal domain [e.g., *McKee et al.* 1969; *Mill and Drayson* 1978; *Goldman and Saunders* 1979; *Carlotti* 1988; *Ridolfi et al.* 2000; *von Clarmann et al.* 2003; *Raspollini et al.* 2006]. Because of horizontal variations of the real atmospheric state, this assumption causes a so-called smoothing error [*Rodgers*, 2000] and affects the horizontal resolution of the limb measurement. This horizontal smoothing must be considered in quantitative applications, e.g. in comparisons of measurements with modeled data, data assimilation [e.g., *Lahoz et al.* 2007], whenever the model grid is significantly finer than the horizontal resolution of the measurement. Similar considerations apply to the intercomparison of measurements of different horizontal resolution [e.g., *Ridolfi et al.* 2007]. In this paper we present a set of horizontal averaging kernels for Michelson Interferometer for Passive Atmospheric Sounding (MIPAS) [*Fischer et al.*, 2008]. These averaging kernels characterize the horizontal response of the retrieval to a delta perturbation of the true atmospheric state [*Rodgers*, 2000]. In particular, they can be used to construct horizontal observation operators [c.f., *Ide et al.* 1997].

5.9 MIPAS measurements and retrievals

MIPAS is an infrared limb emission sounder on Envisat, designed and operated for measurements of constituents between the upper troposphere and the mesosphere. MIPAS is a rear looking instrument with the lines of sight approximately in the orbit plane. In the original measurement mode, which was operational from July 2002 to March 2004, 17 tangent altitudes between 6 and 68 km were measured per limb scan. The altitude of the Envisat orbit is about 800 km, and the ground track speed is about 510 km per 76.5 s which are needed to record one full limb scan. The field of view covers about 3 km in altitude at the tangent point. The horizontal extension of the field of view is about 30 km at the tangent point. While the latter number indicates the horizontal extension of the air mass sampled by MIPAS, it is not adequate to talk about cross-track resolution here, because there is no instantaneous cross-track sampling.

The operational MIPAS level-2 processor [*Ridolfi et al.*, 2000; *Raspollini et al.*, 2006] performs a maximum likelihood profile retrieval [*Rodgers*, 2000] of temperature and trace species abundance profiles using an unconstrained global fit approach [*Carlotti*, 1988]. As usual in limb sounding, horizontal homogeneity of the atmosphere is assumed. The vector y contains those measurements of a MIPAS limb scan which are actually used for the retrieval [*Dudhia et al.*, 2002; *Raspollini et al.*, 2006] of the vertical profile x of the target variable, sampled at the tangent altitudes of the limb measurements, K is the Jacobian matrix containing the partial derivatives $\partial y_m/\partial x_n$. S_y is the measurement noise covariance matrix. The estimate $\hat{x}$ of the vertical profile of the target variable can be calculated as

$$\hat{x}_{i+1} = \hat{x}_i + \left(K^T S_y^{-1} K + \lambda I\right)^{-1} K^T S_y^{-1} (y - F(\hat{x}_i)), \tag{5.17}$$

where i is the iteration number in a Newtonean iteration, and F is the radiative transfer model used for simulation of the measurements. The term λI limits the stepwidth of the iteration and pushes the correction vector $x_{i+1} - x_i$ towards the direction of the steepest gradient of the penalty

function $(y-F(x))^T S_y^{-1}(y-F(x))$ [*Levenberg*, 1944; *Marquardt*, 1963] but does not influence the solution in the case perfect numerical convergence is achieved. This term thus does not need to be considered in estimating the spatial response function of the retrieval. As most common limb retrieval schemes, Eq. 5.17 assumes local horizontal homogeneity of the atmosphere. The vertical averaging kernel of this kind of retrieval, i.e. the derivative of the estimated profile with respect to the true atmospheric state, sampled on the tangent altitude grid, is unity. The horizontal averaging kernels need some further investigation.

5.10 Horizontal averaging kernels: theory

In order to allow the assessment not only of hard-wired 1-D retrievals but also of retrievals where horizontal variability is subject to a soft constraint, we formulate this retrieval as a formal two-dimensional retrieval (altitude and along-track coordinate) where the assumption of horizontal homogeneity is implemented by a numerical constraint. For clarity, we omit all formalism related to the Newtonean iteration because this is unnecessary for retrieval diagnostics in the case of moderately nonlinear radiative transfer. We further assume that the lines of sight of the instrument lie in the orbit plane of the spacecraft, an assumption which is justified for major parts of the Envisat orbit [*Carlotti et al.*, 2001]:

$$\hat{x}_{2\mathrm{D}} = \hat{x}_{2\mathrm{D},0} + \left(K_{2\mathrm{D}}^T S_y^{-1} K_{2\mathrm{D}} + R\right)^{-1} K_{2\mathrm{D}}^T S_y^{-1}(y - F(x_{2\mathrm{D},0})) \tag{5.18}$$

Here $x_{2\mathrm{D}}$ is the 2-dimensional representation of the atmospheric state, arranged in a column vector $(x_{1,1},\ldots,x_{1,j},x_{2,1},\ldots,x_{2,j},\ldots,x_{k,j})^T$ where k is the number of altitude gridpoints and j is the number of horizontal gridpoints (in a geocentered angular coordinate). The Jacobian $K_{2\mathrm{D}}$ contains the derivatives of the signal with respect to the full 2-dimensional field of atmospheric state variables, as provided by radiative transfer codes supporting 2-dimensional radiative transfer and Jacobian calculation, e.g. the KOPRA model [*Steck et al.*, 2005; *Stiller*, 2000; *Stiller et al.*, 2002] or the forward model used in the Geo-fit [*Carlotti et al.*, 2001] or the GMTR [*Carlotti et al.*, 2006] retrieval codes. The $jk \times jk$ constraint matrix R is block-diagonal. Each diagonal block of the size $k \times k$ is calculated as $\gamma L^T L$ where L is a first order finite differences operator [*Phillips*, 1962; *Tikhonov*, 1963a,b; *Twomey*, 1963, 1965]:

$$L = \begin{pmatrix} -1 & 1 & 0 & \ldots & 0 & 0 \\ 0 & -1 & 1 & \ldots & 0 & 0 \\ & & & \ddots & & \\ 0 & 0 & 0 & \ldots & -1 & 1 \end{pmatrix} \tag{5.19}$$

With the scalar tuning parameter γ chosen large enough, all horizontal variation of the atmosphere is suppressed and a 1-dimensional profile retrieval is emulated within the 2-dimensional retrieval formalism. Differentiation of Eq. 5.18 with respect to the the true atmospheric state $x_{2\mathrm{D}}$ gives the 2-dimensional averaging kernel of the 1-dimensional retrieval:

$$A_{2\mathrm{D}} = \left(K_{2\mathrm{D}}^T S_y^{-1} K_{2\mathrm{D}} + R\right)^{-1} K_{2\mathrm{D}}^T S_y^{-1} K_{2\mathrm{D}} \tag{5.20}$$

The k diagonal blocks of size $j \times j$ of the $kj \times kj$ averaging kernel are the horizontal averaging kernels of the retrieval. With γ large enough to remove all horizontal variation, all the rows

within such a block are identical. A row of a diagonal block can be used as horizontal observation operator at the respective altitude and can be used to characterize the horizontal smoothing of a standard 1-dimensional limb retrieval.

For hard-wired one-dimensional profile retrievals, the horizontal averaging kernel can be obtained in a more straight-forward manner simply by differentiating the one-dimensional estimates (i.e. the vertical profile values) with respect to the variations of the true two-dimensional field of atmospheric state variables.

$$A_{\mathrm{hor}} = \left(K^T S_y^{-1} K\right)^{-1} K^T S_y^{-1} K_{\mathrm{2D}} \tag{5.21}$$

Applied to hard-wired one-dimensional profile retrievals evaluated for a horizontally homogeneous atmosphere, the approaches Eq. 5.20 and Eq. 5.21 are equivalent with respect to the result but Eq. 5.21 is computationally more efficient. Results are different for averaging kernels evaluated for a non-homogeneous atmosphere because non-homogeneity is considered in the Jacobian K_{2D} of Eq. 5.20 but not in the Jacobian K used in Eq. 5.21. In such cases, the latter approach is appropriate to characterize hard-wired one-dimensional retrievals, while the former characterizes constrained two-dimensional retrievals.

5.11 Application to MIPAS

Horizontal averaging kernels have been calculated for the MIPAS key products (temperature and mixing ratios of H_2O, O_3, CH_4, N_2O, HNO_3 and NO_2). These horizontal averaging kernels refer to MIPAS high spectral resolution (0.025 cm^{-1}, unapodized) measurements that were acquired from July 2002 until March 2004. These calculations are based on Jacobians calculated with the KOPRA [*Stiller*, 2000] radiative transfer model with 50 km horizontal gridwidth and a vertical retrieval grid defined by the MIPAS nominal tangent altitudes (6-42 km at 3-km stepwidth, additionally 47, 52, 60 and 68 km, reduced altitude range for some species). These calculations have been performed for a retrieval setup consistent with the MIPAS offline (OFL) data [*Raspollini et al.*, 2006], which cover a wider altitude range and are based on a larger subset of the available tangent altitudes than the MIPAS near-real-time (NRT) data. Three atmospheric conditions have been investigated (Figure 5.13), namely midlatitudinal, polar, and tropical [*Kiefer et al.*, 2002]. Unless explicitly mentioned, the Jacobians were evaluated for a horizontally homogeneous atmosphere. No numerical constraint has been applied in the vertical except that implied by the quite coarse retrieval grid.

We discuss the results with respect to three characteristics, namely information displacement, information spread, and impacts onto the profile shape. Numerical results for quantitative use are provided in the supplemental data (http://www.atmos-meas-tech.net/2/47/2009/amt-2-47-2009-supplement.zip). In this paper we restrict the discussion to some typical sample cases.

5.11.1 Information displacement

The information displacement we define is the horizontal distance between the point where the most information comes from and the nominal geolocation of the limb scan, which is defined as the geolocation of the tangent point of the middle line of sight in a MIPAS limb scan. For a nominal

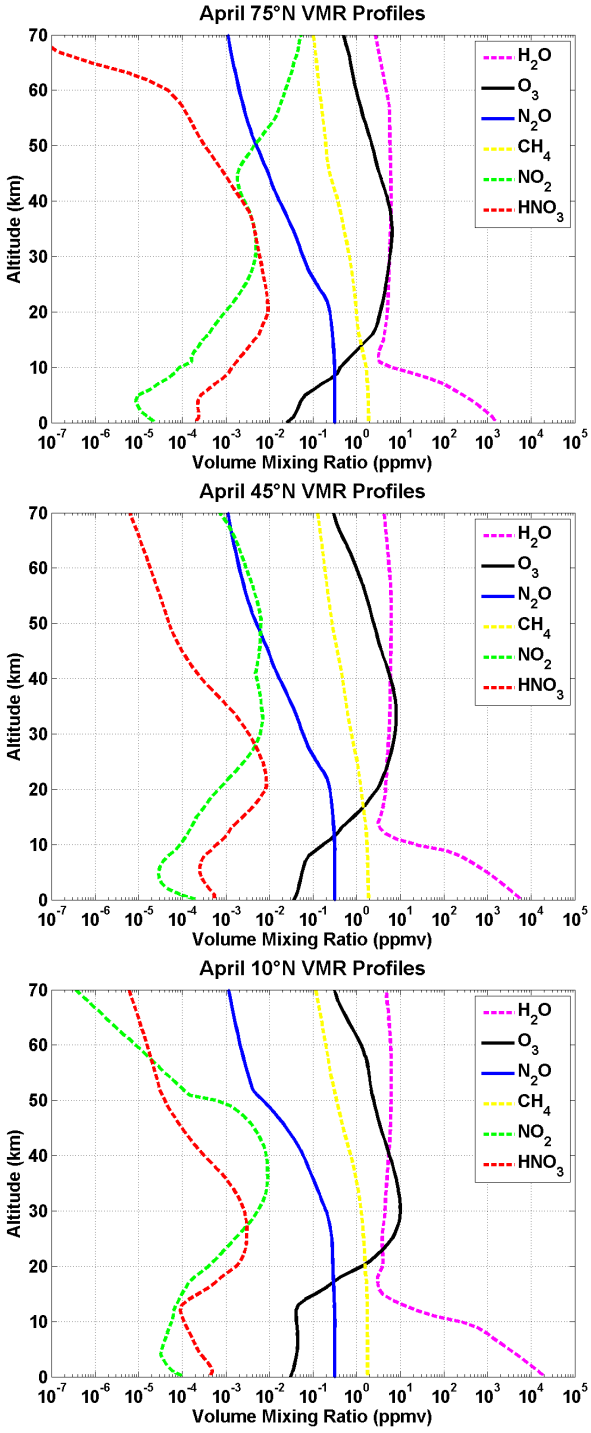

Figure 5.13: Target species mixing ratio vertical profiles used in this study for polar (top panel), milatitude (middle panel) and tropic (lower panel) atmospheres.

MIPAS limb scan this is the geolocation of the 30-km tangent point. The ESA online processor assumes local horizontal homogeneity and each retrieved profile is assigned to the nominal geolocation of the limb scan.

A part of the information displacement is explained by the observation geometry and the satellite movement, but radiative transfer effects and sampling density are also important in some cases. The information displacement can be calculated on the basis of the position of the centroid of the horizontal averaging kernel, its maximum or the median. All these quantifiers are reported in the in the supplemental data files (http://www.atmos-meas-tech.net/2/47/2009/amt-2-47-2009-supplement.zip).

The tangent point is displaced towards the satellite by 160 km for the lowermost nominal tangent altitude (6 km) and 159 km in the opposite direction for the uppermost nominal tangent altitude (68 km). This displacement is caused by the satellite movement ($\approx$ 510 km per limb scan) and the position of the tangent point as a function of the elevation angle. Since MIPAS is rearward looking top down scanning, both effects in tendency compensate, with a net movement of the tangent point of about 320 km during one limb scan in flight direction. In most trace gas retrievals, this geometrically caused displacement explains the majority of the actual information displacement for all species and most altitudes. Figure 5.14 shows the O_3 midlatitudes horizontal averaging kernels and may serve as a typical example. Besides this displacement due to measurement geometry, in most cases the information maximum is displaced slightly (typically less than 10 km) towards the satellite. The latter is because weighting functions of a single line of sight through a horizontally homogeneous atmosphere typically peak between the tangent point and the satellite because of the nonlinearity of radiative transfer. A longer optical path between the emitting air volume and the observing instrument goes along with more absorption of the signal. The only exceptions are H_2O (all atmospheres) and CH_4 (tropical and midlatitudinal atmospheres) at the uppermost altitude of 68 km. Since the particular retrieval scheme under assessment scales the a priori profiles above the uppermost tangent altitude instead of attempting to obtain independent profile information, this altitude represents the information about the entire atmosphere between 68 km and the top of the atmosphere [c.f. *Ridolfi et al.* 2000 or *Raspollini et al.* 2006]. In these particular cases the peak of information is displaced by up to about 510 km towards the satellite (Fig. 5.15). This is because in these cases the information gained through emission of radiance near the tangent point is outweighted by absorption in higher, colder atmospheric layers. This effect is particularly large in cases of non-linear radiative transfer in an atmosphere of large opacity in the given spectral region.

In some cases, however, the majority of information of MIPAS profile retrievals originates from the atmosphere slightly beyond the actual tangent point, e.g. for daytime tropical NO_2 at 42 and 50 km altitude (Figure 5.16). While the argument of nonlinear radiative transfer certainly holds for each single MIPAS limb scan, this effect can sometimes be overcompensated for all but the lowermost tangent altitudes by the following geometrical effects: First, the MIPAS field of view is finite and covers about 3 km in the vertical at the tangent point. This means that beyond the tangent point the fields of view of measurements at adjacent tangent altitudes are overlapping, leading to multiple sampling of air masses beyond the tangent point. This effect accounts for a backward displacement of the median point by 1-7 km. Moreover, the interaction between satellite movement and downward scanning contributes to this effect: While a limb sequence of spectra is recorded top down, i.e. from the uppermost to the lowermost tangent altitude, Envisat moves about 510 km in the opposite of the viewing direction. This leads, during one single limb scan, to

denser sampling of the atmosphere beyond the tangent points than satellite-side of the tangent point. Through the satellite motion, the points where the raypaths of a limb scan intersect a certain altitude level move together beyond the tangent point, while they diverge on the satellite side of the tangent point. As a consequence, the retrieval uses more information per latitude increment from beyond the tangent point (c.f. Figure 5.15, 30 km altitude). This explanation has been verified by a test retrieval where the satellite was assumed stationary and where this information displacement effect has not been observed. Due to its small effect, however, this issue is of purely academic interest.

For temperature the situation is slightly different: Most information on temperature originates from a point displaced from the actual tangent point towards the satellite by about 50 to 100 km (Figure 5.17). This is because at the spectral intervals used for temperature retrieval the atmosphere is far less transparent than at those used for trace gas abundance retrievals. This is an issue not only because the temperature information is inaccurately assigned to its true geolocation but also because this can trigger a systematic error when retrieved temperatures are subsequently used for trace gas retrievals. While this kind of error is included in the error budget of the MIPAS-OFL data [*Raspollini et al.*, 2006], other MIPAS data processors account for this problem by retrieving a horizontal temperature gradient jointly with the temperature and elevation pointing and using this gradient information for subsequent trace gas retrievals (c.f. http://imk.fzk.de/asf/ame/envisat-data).

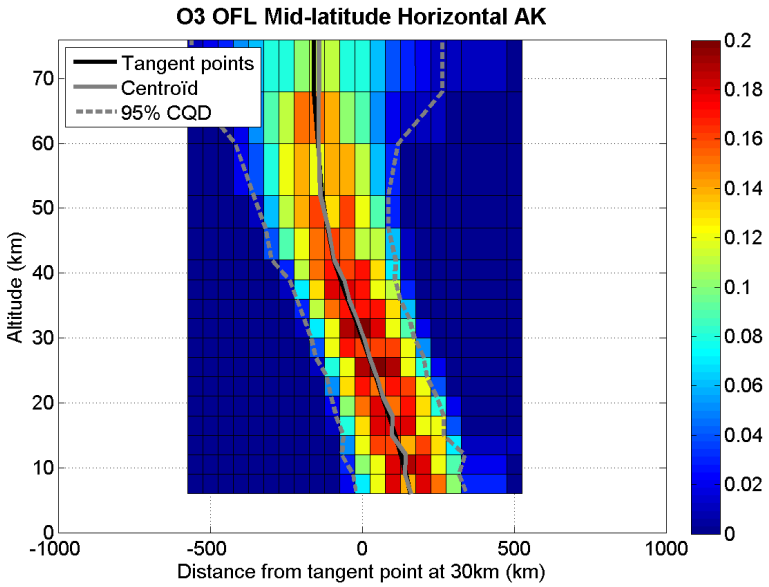

Figure 5.14: MIPAS horizontal averaging kernel for O_3, evaluated for a midlatitude homogeneous atmosphere. The black line is the position of the actual tangent points. The grey line is the centroid of the horizontal averaging kernel. 90% of the information originates from the region between the dashed lines. Negative distances are displacement towards beyond the tangent point, positive distances are displacement towards the satellite. Numeric data are found in the auxiliary files.

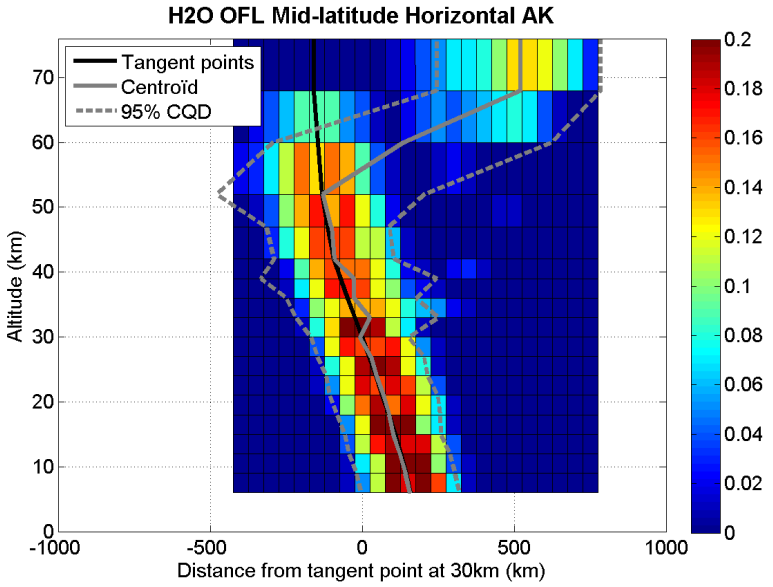

Figure 5.15: MIPAS horizontal averaging kernel for H_2O, evaluated for a midlatitude homogeneous atmosphere. For details, see Figure 5.14. Pronounced information displacement towards the satellite through saturized radiative transfer is visible for the uppermost altitudes.

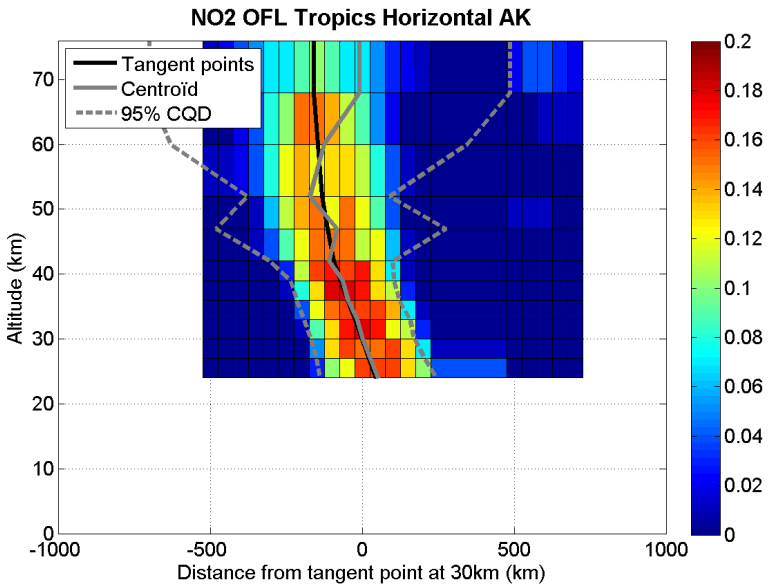

Figure 5.16: MIPAS horizontal averaging kernel for NO_2, evaluated for a tropical daytime homogeneous atmosphere. For details, see Figure 5.14. Some minor information displacement towards beyond the tangent point is visible near 42 and 50 km altitude.

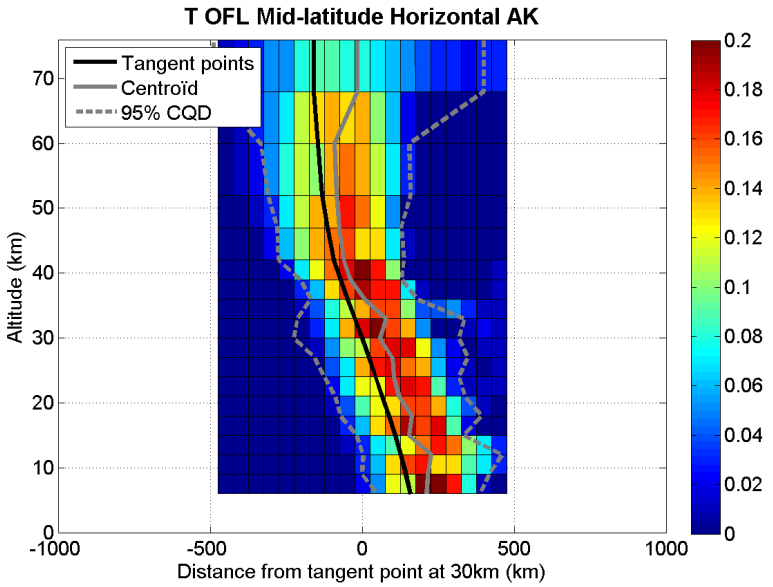

Figure 5.17: MIPAS horizontal averaging kernel for temperature, evaluated for a mid-latitude homogeneous atmosphere. For details, see Figure 5.14. There is a systematic information displacement of 50–100 km towards the satellite.

5.11.2 Information spread

The information spread is a measure of the horizontal smearing of the retrieval. We report the spread in terms of both the half-width (full width at half maximum, FWHM) and various centered quantile distances (CQD), namely 50%, 68%, 95%, and 99%. The x% CQD is the distance between the $x + (1 - x)/2$ and the $(1 - x)/2$ quantiles and indicates the horizontal region x percent of information originates from.

The FWHM of the horizontal averaging kernel generally increases with altitude. It ranges from 210 km (CH_4, tropical atmosphere) to 330 km (NO_2, tropical atmosphere daytime) at 6 km tangent altitude. The respective 95% CQDs are 262 km and 382 km. For 52 km tangent altitude, it ranges from 315 km (H_2O, midlatitudes) to 387 km (N_2O, polar atmosphere), with related 95-% CQDs of 683 km (H_2O, midlatitudes) and 478 km (N_2O, polar atmosphere). The FWHM is somewhere between the 68-% and the 95-% CQDs in most cases. Compared to the MIPAS along-track sampling, which is about 510 km, the horizontal smearing in terms of FWHM often is a factor of about 2 smaller. That means that the atmosphere is horizontally undersampled even in the along-track direction. In consequence, small-scale periodic phenomena are prone to aliasing.

5.11.3 Impact of horizontal smoothing on profile information

In order to assess if the horizontal smoothing error triggers profile errors, in other words, to find out if the hard constraint of horizontal homogeneity causes profile errors, we have calculated the

horizontally integrated averaging kernel $\tilde{A}$ with the elements

$$\tilde{a}_{k,n} = \sum_{i=1}^{j} a_{i;k,n} \tag{5.22}$$

where k and n are the altitude indices and i is the horizontal index of the element a of A_{hor}. $\tilde{A}$ was found to equal the identity matrix at at least three digits. This confirms expectations that within linear estimation no profile error is triggered by horizontal smoothing and verifies the implementation of the method.

5.11.4 Averaging kernels evaluated for horizontally non-homogeneous atmospheres

The horizontal averaging kernels discussed above were evaluated for horizontally homogeneous atmospheres. One might expect different behaviour of retrievals in horizontally inhomogeneous atmospheres. Temperature is a particularly critical parameter whose horizontal gradients may largely affect radiative transfer. Horizontal gradients in interfering trace species are supposed to have small influence due to efficient microwindow selection, where interferences by non-target species are minimized. Thus we have, as a kind of estimate for a particularly difficult case, evaluated the horizontal averaging kernel for a midlatitudinal ozone retrieval in an atmosphere with an along-line-of-sight temperature gradient of 1K/100km, increasing from North to South. Results do not largely differ from those evaluated for the horizontally homogeneous atmosphere (Figure 5.18). The FWHM is smaller by less than 2.5%, and the center of information is moved by only about 5 km off the satellite.

As a worst case, we have also investigated the horizontal averaging kernel evaluated for an atmosphere with a horizontal temperature gradient of 10K/100 km, applicable over a range of 400 km around the nominal geolocation of the limb scan, i.e. with a maximum temperature difference of 40 K between the colder foreground and the warmer background. While the information spread is not significantly affected, there is an information displacement of about 50 km towards the background (Figure 5.19). Due to higher temperatures beyond the tangent point, radiance contributions and thus Jacobians are larger there.

We conclude that it is justified to use the averaging kernels evaluated for homogeneous atmospheres as approximative averaging kernels for the true atmospheric state, unless extreme horizontal temperature gradients are analyzed using models with horizontal gridwidth approaching 50 km.

5.12 Conclusions

The horizontal MIPAS averaging kernels indicate the region where the retrieved profile information originates from and describe the horizontal smoothing of a retrieval which assumes local horizontal homogeneity of the atmospheric state. The latitudinal smearing of information is surprisingly small (below about 380 km in terms of FWHM, below about 500 km in terms of CQD except for the uppermost altitudes) and is considerably smaller than the horizontal sampling (ca. 510 km) which is defined by the horizontal distance between two adjacent limb scans. This means that the atmosphere is not continuously sampled by the MIPAS nominal high resolution measurement

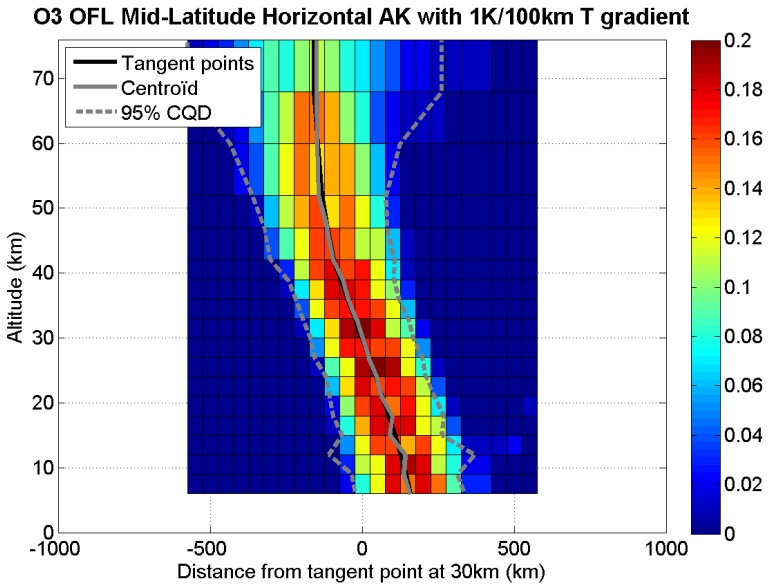

Figure 5.18: MIPAS horizontal averaging kernel for O_3, evaluated for a midlatitude atmosphere with a meridional temperature gradient of 1K/100km, warmer towards South. For details, see Figure 5.14.

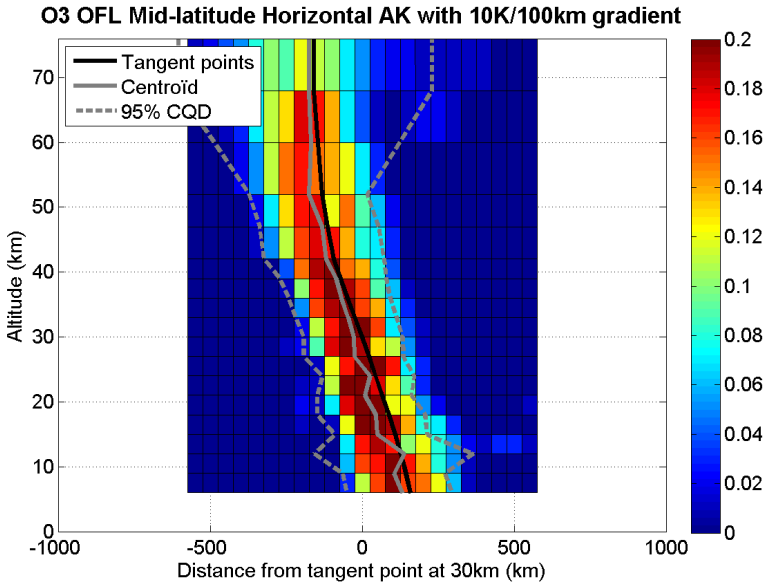

Figure 5.19: MIPAS horizontal averaging kernel for O_3, evaluated for a meridional temperature gradient of 10K/100km, applicable over a range of 400 km, warmer towards South. For details, see Figure 5.14.

scenario. A potential consequence of this along-track undersampling and missing physical low-pass filtering by the measurement geometry is the risk of aliasing effects even in the along-track direction when small scale wave structures are analyzed.

The horizontal MIPAS averaging kernels can be used to construct the along-track components of observation operators for data assimilation purposes. The low horizontal sampling width allows to disregard the horizontal smearing effects of MIPAS for all assimilation or model comparison applications where the horizontal gridwidth is larger than about 300 km. For many of these applications, it will be sufficient to just consider the information displacement relative to the nominal geolocation of the MIPAS limb scan. With a few exceptions, the horizontal displacement is dominated by the displacement of the tangent point with respect to the nominal geolocation of the limb scan, while other effects (nonlinearity of radiative transfer, overlapping fields of view behind the tangent point, and denser sampling behind the tangent point) play a minor role, except for temperature, where the information is displaced by 50–100 km from the actual tangent point towards the satellite. In the cross-track domain, MIPAS data can be interpolated like point-measurements unless the model gridwidth approaches values as low as 30 km, which is the horizontal width of the instantaneous field of view of MIPAS.

While the numerical values presented here are MIPAS instrument-specific, and even depend on the MIPAS measurement scenario (results shown here refer to the nominal high spectral resolution measurement mode), the methods to calculate the horizontal averaging kernels can be applied to each limb sounding emission or occultation instrument with lines of sight approximately in the orbit plane, and, with straight-forward modifications, also to any other limb sounding instrument. An application of this approach to constrained retrievals is found in *von Clarmann et al.* [2009].

Acknowledgements. This work has been funded by EC FP6 Integrated Project GEOMon (contract 036677), ProDEx project SECPEA and ESA MIPAS QWG.

General conclusion and recommendations

A new method has been proposed to characterise the horizontal resolution and extent of MIPAS atmospheric profile data. For this rear-viewing limb scanning sounder, the across-track resolution is determined at first order by the IFOV, which is 30 km at tangent point. The along-track resolution results from concurring geometrical and radiative effects and retrieval properties and is not straightforward to determine.

The first part of this analysis is dedicated to the analysis of the radiative and geometrical effects at the origin of the measured radiance signal. The horizontal along-track contribution to total radiance has been calculated using a simplified radiative transfer model. The study concludes that the portion of the optical path that contributes to the measurement may extend over more than 1000 km, depending on the tangent altitude. The contribution to radiance along the line-of-sight has a complex shape and its maximum does not occur at the tangent point. This part of the study considers only on the physics of the radiative transfer in the atmosphere. It does not take into account instrumental and retrieval characteristics. Therefore, the second part of the analysis focuses on the characterisation of the horizontal resolution of a full retrieval system. A method has been developed and applied to MIPAS to calculate adequate two-dimensional averaging kernels (altitude and along-track coordinate). According to the study of the horizontal component of the two-dimensional kernels, the actual along-track smearing of the retrieved information is surprisingly small, below about 380 km for FWHM and slightly larger for the 95% (2σ) centered quantile difference of the captured information. The along-track sampling is defined by the horizontal distance between two adjacent limb scan sequences, ca. 510 km more or less in the North-South direction. It is thus larger than the along-track resolution. With twice daily (night and day) sampling of the atmosphere by 14.3 orbits a day and an across-track IFOV of 30 km, the longitude sampling varies with latitude, yielding daily a zonal coverage of about 6% at the polar circles but only 2.5% at the equator. A potential consequence of both the along-track and longitude undersampling, and of missing physical low-pass filtering by the measurement geometry, is the risk of aliasing effects even in the along-track direction when small scale wave structures are analyzed.

Horizontal characteristics of the retrieved MIPAS profile data have consequences for applications implying comparisons of MIPAS data with other observations (e.g. geophysical validation) and with modelling results (e.g. ingestion in data assimilation systems). A first aspect is the along-track displacement of the retrieved information. With a few exceptions, the horizontal displacement is dominated by the displacement of the tangent point with respect to a fixed reference, e.g. the geolocation of the tangent point at 30 km altitude, while other effects (nonlinearity of

radiative transfer, overlapping fields of view behind the tangent point, and denser sampling behind the tangent point) play a minor role. Temperature constitutes an exception: the information is displaced by 50-100 km from the actual tangent point towards the satellite. For satellite validation using ground-based observations, the severe asymmetry of the MIPAS air masses suggest to preferably use geographical collocation criteria based on across-track and along-track distances rather than the radius around the ground station. A second aspect is the horizontal resolution of the retrieved data. For most of current chemistry-transport models and assimilation systems, the latitude step, typically 2.5° to 5°, is close to or much larger than the horizontal resolution of MIPAS, and MIPAS smoothing effects can be neglected. For higher resolution models and systems as currently under development, the horizontal MIPAS averaging kernels presented here can be used to construct an observation operator of information along-track. The across-track operator may remain a simple interpolation as long as the model grid resolution does not get close to 30 km.

While the numerical values presented here are MIPAS instrument-specific, and even depend on the MIPAS measurement scenario (results shown here refer to the nominal high spectral resolution measurement mode), the methods to calculate the horizontal averaging kernels and the principles of the discussion can be applied to each limb sounding instrument with lines of sight approximately in the orbit plane, and, with straight-forward modifications, also to any other limb sounding instrument.